PROCEEDINGS OF THE IEEE, VOL. 62, NO. 11, NOVEMBER 1974

A Uniform Geometrical Theory of Diffraction for an Edge in a Perfectly Conducting Surface

ROBERT G. KOUYOUMJIAN, SENIOR MEMBER, IEEE, AND PRABHAKAR H. PATHAK

Abstract—A compact dyadic diffraction coefficient for electromagnetic waves obliquely incident on a curved edge formed by perfectly conducting curved or plane surfaces is obtained. This diffraction coefficient remains valid in the transition regions adjacent to shadow and reflection boundaries, where the diffraction coefficients of Keller's original theory fail. Our method is based on Keller's method of the canonical problem, which in this case is the perfectly conducting wedge illuminated by plane, cylindrical, conical, and spherical waves. When the proper ray-fixed coordinate system is introduced, the dyadic diffraction coefficient for the wedge is found to be the sum of only two dyads, and it is shown that this is also true for the dyadic diffraction coefficients of higher order edges. One dyad contains the acoustic soft diffraction coefficient; the other dyad contains the acoustic hard diffraction coefficient. The expressions for the acoustic wedge diffraction coefficients contain Fresnel integrals, which ensure that the total field is continuous at shadow and reflection boundaries. The diffraction coefficients have the same form for the different types of edge illumination; only the arguments of the Fresnel integrals are different. Since diffraction is a local phenomenon, and locally the curved edge structure is wedge shaped, this result is readily extended to the curved wedge. It is interesting that even though the polarizations and the wavefront curvatures of the incident, reflected, and diffracted waves are markedly different, the total field calculated from this high-frequency solution for the curved wedge is continuous at shadow and reflection boundaries.

I. Introduction

THIS PAPER is concerned with the construction of a high-frequency solution for the diffraction of an electromagnetic wave obliquely incident on an edge in an otherwise smooth curved perfectly conducting surface surrounded by an isotropic homogeneous medium. The surface normal is discontinuous at the edge, and the two surfaces forming the edge may be convex, concave, or plane. The solution is developed within the context of Keller's geometrical theory of diffraction (GTD) [1]–[3] so the dyadic diffraction coefficient is of interest. Particular emphasis is placed on finding a compact accurate form of the diffraction coefficient valid in the transition regions adjacent to shadow and reflection boundaries and useful in practical applications. In treating this problem the wedge was considered first; its solution was extended later to the curved wedge.[1]

According to the GTD, a high-frequency electromagnetic wave incident on an edge in a curved surface gives rise to a reflected wave, an edge diffracted wave, and an edge excited wave which propagates along a surface ray. Such surface ray fields may also be excited at shadow boundaries of the curved surface. The problem is easily visualized with the aid of Fig. 1, which shows a plane perpendicular to the edge at the point of diffraction Q_E. The pertinent rays and boundaries are projected onto this plane. To simplify the discussion of the reflected field, we have assumed that the local interior wedge angle is $\leqslant \pi$. According to Keller's generalized Fermat's principle, the ray incident on the edge Q_E produces edge diffracted rays *ed* and surface diffracted rays *sr*. In the case of convex surfaces, the surface ray sheds a surface diffracted ray *sd* from each point Q on its path. *ES* is the boundary between the edge diffracted rays and the surface diffracted rays; it is tangent to the surface at Q_E. *SB* is the shadow boundary of the incident field and *RB* is the shadow boundary of the reflected field, referred to, henceforth, simply as the reflection boundary. If both surfaces are illuminated, then there is no shadow boundary at the edge; instead there are two reflection boundaries for the problem considered here. Since the behavior of the ray optics field is different in the two regions separated by a boundary, there is a transition region adjacent to each boundary within which there is a rapid variation of the field between the two regions.

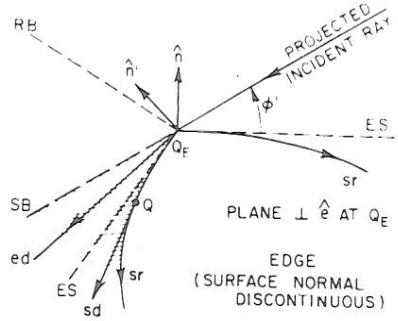

Fig. 1. Incident, reflected, and diffracted rays and their associated shadow and reflection boundaries projected onto the plane normal to the edge at the point of diffraction Q_E.

In the present analysis it is assumed that the sources and field point are sufficiently removed from the surface and the boundary *ES* so that the contributions from the surface ray field can be neglected. The total electric field may then be represented as

$$E = E^i u^i + E^r u^r + E^d. \tag{1}$$

In which E^i is the electric field of the source in the absence of the surface, E^r is the electric field reflected from the surface with the edge ignored, and E^d is the edge diffracted electric field. The functions u^i and u^r are unit step functions which are equal to one in the regions illuminated by the incident and reflected fields and to zero in their shadow regions. The extent of these regions is determined by geometrical optics. The step functions are shown explicitly in (1) to emphasize the discontinuity in the incident and reflected fields at

Manuscript received July 3, 1974; revised August 1, 1974. The initial work on the solutions of the canonical problems was supported in part by Contract AF 19(628)-5929 between Air Force Cambridge Research Laboratories and The Ohio State University Research Foundation; the subsequent work on the generalization of these solutions was supported in part by Grant NGR 36-008-144 between NASA and The Ohio State University Research Foundation.

The authors are with the ElectroScience Laboratory and the Department of Electrical Engineering, Ohio State University, Columbus, Ohio 43212.

[1] The term "curved wedge" is used when one of the surfaces forming the edge is curved.

the shadow and reflection boundaries, respectively. They are not included in subsequent equations for reasons of notational economy.

The diffracted field as defined by (1) penetrates the shadow region, which according to geometrical optics, has a zero field to account for the nonvanishing fields known to exist there. But the correct high-frequency field must be continuous at the shadow and reflection boundaries; hence the diffracted field must also compensate for the discontinuities in the incident and reflected fields there. In other words, the diffracted field must provide the correct transition between the illuminated regions and the regions shadowed by the edge.

The high-frequency solution described in the next sections is obtained in the following way. A Luneberg–Kline expansion [4] for the incident field is assumed to be given. The reflected field is expanded similarly and related to the incident field by imposing the boundary condition at the perfectly conducting surface. Only the leading term is retained. Next the general form of the leading term in the high-frequency solution for the edge diffracted electromagnetic field is determined. The wedge (formed by the intersection of two plane surfaces) is treated first; its dyadic diffraction coefficient is deduced from the asymptotic solution of several canonical problems. Some parameters in this diffraction coefficient are seen to depend on the type of edge illumination. They are determined for an arbitrary incident wavefront by requiring the leading term in the total field to be continuous at the shadow and reflection boundary. It is found that only a slight extension of the solution for the wedge is needed to treat the more general problem posed by the curved edge.

This paper follows in a natural way from some earlier work. In [5] the Pauli–Clemmow method of steepest descent was employed in a manner different from that employed by Pauli [6] to obtain a more accurate asymptotic solution for the field diffracted by a wedge. We showed that our generalized Pauli expansion can be transformed term by term into a generalized form of the asymptotic expansion given by Oberhettinger [7]. The leading term in our expansion was found to be more accurate than the leading term in Oberhettinger's expansion; furthermore, our leading term for the diffracted field contains a simple correction factor, which permits the field to be calculated easily in the transition region. This property is of considerable practical importance, because it enables one to use the GTD in the transition regions without introducing a supplementary solution. The correction factors, referred to here as transition functions, are simply included with the diffraction coefficient.

In [5] only the scalar problem of plane waves normally incident of the edge of the wedge is considered. In [8], this work is extended to obtain a dyadic diffraction coefficient for a perfectly conducting wedge illuminated by obliquely incident plane, conical, and spherical waves. By introducing the natural ray-fixed coordinates, the dyadic diffraction coefficient obtained from each of these canonical problems is reduced to the sum of two dyads. In other words, the matrix formed by the elements of the dyadic diffraction coefficient is a two by two diagonal matrix. The diagonal elements of this matrix are simply the scalar diffraction coefficients D_h and D_s for the Neumann (hard) and Dirichlet (soft) boundary conditions, respectively. The transition functions appearing in D_s and D_h have the same form for the four types of illumination; in each case only a Fresnel integral is involved. However, the argument of the Fresnel integral depends upon the type of illumination. Outside of the transition regions these factors are approximately one, and Keller's expressions for the diffraction coefficients are obtained. The asymptotic solutions described in this paragraph help us formulate the solution for a more general type of illumination of the wedge, as noted earlier.

The analysis of wedge diffraction has had a lengthy history. Only a few of the reports and papers have been mentioned thus far. Many of the more important papers on this subject may be found in [9] and [10]. A good review of wedge diffraction and the special case of half-plane diffraction is given in [9, chs. 6 and 8]. Recently, Ahluwalia, Boersma, and Lewis have written some papers [11]–[13] of special relevance to the work described here. In [11] and [12] high-frequency asymptotic expansions for scalar waves diffracted by curved edges in plane and curved screens are described, and this work is extended to a curved edge in a curved surface in [13]. The authors make use of ray coordinates, and some of their results dealing with rays and wavefronts have been helpful in the development of our solution. Nevertheless, there are some noteworthy differences between their solutions and ours, apart from the fact that their problem is scalar instead of the vectorial problem treated here. Their formulation or ansatz begins with the total field, and the resulting correction of the ordinary GTD solution in the transition region is different from ours. Our result is related more directly to the form of the GTD solution; furthermore, it appears to be more accurate when only the leading term in the two asymptotic expansions is retained.

II. The Geometrical-Optics Field

The geometrical-optics field, which is the sum of the leading terms in the asymptotic expansions for the incident and reflected fields, is a part of our high-frequency solution for edge diffraction. The incident and reflected electric fields are expanded in Luneberg–Kline series

$$E \sim \exp(-jk\psi) \sum_{m=0}^{\infty} \frac{E_m}{(j\omega)^m} \tag{2}$$

where an $\exp(j\omega t)$ time dependence is assumed and k is the wavenumber of the medium. Substituting the preceding expansion into the vector wave equation for the electric field and integrating the resulting transport equation for $m = 0$ [14], [15], the leading term in (2) is

$$E(s) \sim \exp[-jk\psi(s)]\, E_0(s) = E_0(0) \cdot \exp[-jk\psi(0)] \sqrt{\frac{\rho_1 \rho_2}{(\rho_1 + s)(\rho_2 + s)}} \exp(-jks) \tag{3}$$

which is recognized as the geometrical-optics field. Here s is the distance along the ray path and ρ_1, ρ_2 are the principal radii of curvature of the wavefront at the reference point $s = 0$. In Fig. 2, ρ_1 and ρ_2 are shown in relationship to the rays and wavefronts

It is apparent that when $s = -\rho_1$ or $-\rho_2$, (3) becomes infinite so that it is no longer a valid approximation. The intersection of the rays at the lines 1–2 and 3–4 of the astigmatic tube of rays is called a caustic. As we pass through a caustic in the direction of propagation the sign of $\rho + s$ changes and the correct phase shift of $+\pi/2$ is introduced naturally. Equation (3) is a valid high-frequency approximation on either side of the caustic; the field at a caustic must be found from separate considerations [16], [17].

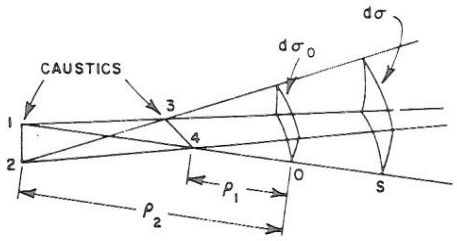

Fig. 2. Astigmatic tube of rays.

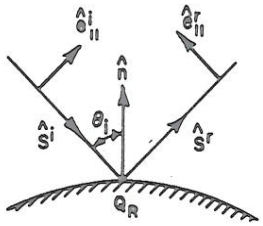

Fig. 3. Reflection at a curved surface.

Employing the Maxwell curl equation $\nabla \times E = -j\omega\mu H$, it follows from (2) that the leading term in the asymptotic approximation for the magnetic field is

$$H \sim Y_c \hat{s} \times E \tag{4}$$

where $Y_c = \sqrt{\epsilon/\mu}$ is the characteristic admittance of the medium, $\hat{s}$ is a unit vector in the direction of the ray path, and E is given by (3). From $\nabla \cdot E = 0$ one obtains

$$\hat{s} \cdot E_0 = 0. \tag{5}$$

Let a high-frequency electromagnetic wave be incident on a smooth curved perfectly conducting surface S, which is part of our curved edge structure. The geometrical-optics electric field reflected at Q_R on S (see Fig. 3) has the form given by (3). Choosing Q_R to be the reference point, it follows from the boundary condition for the total electric field on S that

$$E_0^r(0) \exp[-jk\psi^r(0)] = E^i(Q_R) \cdot \overline{R} = E^i(Q_R) \cdot [\hat{e}_\parallel^i \hat{e}_\parallel^r - \hat{e}_\perp \hat{e}_\perp] \tag{6}$$

in which $E^i(Q_R)$ is the electric field incident at Q_R and $\overline{R}$ is the dyadic reflection coefficient with $\hat{e}_\perp$ the unit vector perpendicular to the plane of incidence and $\hat{e}_\parallel^i$, $\hat{e}_\parallel^r$ the unit vectors parallel to the plane of incidence as shown in Fig. 3. In matrix notation

$$R = \begin{bmatrix} 1 & 0 \\ 0 & -1 \end{bmatrix}. \tag{7}$$

From (3) and (6),

$$E^r(s) = E^i(Q_R) \cdot \overline{R} \sqrt{\frac{\rho_1^r \rho_2^r}{(\rho_1^r + s)(\rho_2^r + s)}} \exp(-jks) \tag{8}$$

in which ρ_1^r and ρ_2^r are the principal radii of curvature of the reflected wavefront at the point of reflection Q_R. The dependence of ρ_1^r and ρ_2^r on the incident wavefront curvature, the aspect of incidence and the curvature of S at Q_R is given Appendix I.

In principle, the geometrical-optics approximations can be improved by finding the higher order terms $E_1^r(R), E_2^r(R), \cdots$, in the reflected field, but in general it is not easy to obtain these from the higher order transport equations. Furthermore, these terms do not correct the serious errors in the geometrical-optics field resulting from the discontinuities at reflection and shadow boundaries.

III. The Edge Diffracted Field

The smooth surface S has a curved edge formed by a discontinuity in its unit normal vector. Equation (3) can be obtained in a quite different way which shows that it is also the leading term in the asymptotic approximation of the diffracted field. Using the method of stationary phase to evaluate the integral representation of the edge diffracted field over its wavefront one obtains

$$E^d(s) \sim E^d(0') \sqrt{\frac{\rho\rho'}{(\rho + s)(\rho' + s)}} \exp(-jks). \tag{9}$$

It is convenient to locate the reference point $0'$ at the edge point Q_E from which the diffracted ray emanates, see Fig. 4; however, the edge is a caustic of the diffracted field. On the other hand, it is clear that $E^d(s)$ given by (9) must be independent of the location of $0'$, hence, $\lim_{\rho' \to 0} E^d(0')\sqrt{\rho'}$ exists. Since the diffracted field is proportional to the field incident at Q_E,

$$\lim_{\rho' \to 0} E^d(0')\sqrt{\rho'} = E^i(Q_E) \cdot \overline{D} \tag{10}$$

where $\overline{D}$ is the dyadic edge diffraction coefficient, which is analogous to the dyadic reflection coefficient of the preceding section. It is assumed here that E^i is not rapidly varying at Q_E, except possibly for its phase variation along the incident ray.

Thus the edge diffracted electric field

$$E^d(s) \sim E^i \cdot \overline{D} \sqrt{\frac{\rho}{s(\rho + s)}} \exp(-jks) \tag{11}$$

in which ρ is the distance between the caustic at the edge and the second caustic of the diffracted ray.

In [25, appendix II], it is shown that

$$\frac{1}{\rho} = \frac{1}{\rho_e^i} + \frac{1}{f} = \frac{1}{\rho_e^i} - \frac{\hat{n}_e \cdot (\hat{s}' - \hat{s})}{a \sin^2 \beta_0} \tag{12}$$

wherein ρ_e^i is the radius of curvature of the incident wavefront at Q_E taken in the plane containing the incident ray and $\hat{e}$ the unit vector tangent to the edge at Q_E, $\hat{n}_e$ is the associated unit normal vector to the edge directed away from the center of curvature, $a > 0$ is the radius of curvature of the edge at Q_E, and β_0 is the angle between the incident ray and the tangent to the edge as shown in Fig. 5(a). The unit vectors $\hat{s}'$ and $\hat{s}$ are in the directions of incidence and diffraction, respectively. Equation (12) is seen to have the form of the elementary mirror and lens formulas in which f is the focal distance. If ρ is positive, there is no caustic along the diffracted ray path; however the caustic distance ρ is negative if the (second) caustic lies between Q_E and the observation point. The diffracted field calculated from (11) is not valid at a caustic, but as one moves outward from Q_E along the diffracted ray, a phase shift of $+\pi/2$ is introduced naturally after the caustic is passed as in the case of the geometrical-optics field.

Since the high-frequency diffracted field has a caustic at the edge, (11) is not valid there, and we cannot impose a condition at Q_E to determine $\overline{D}$ in a manner similar to that used to find

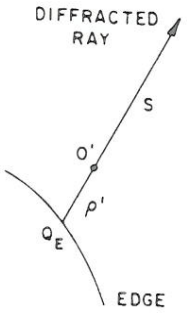

Fig. 4. Edge diffracted ray.

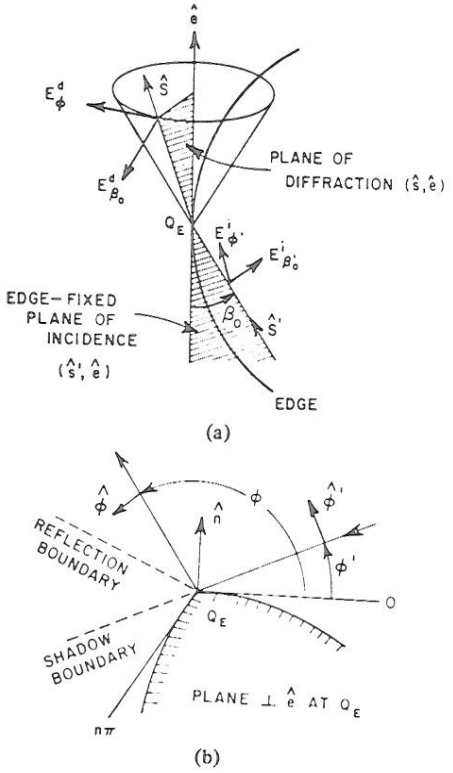

Fig. 5. Diffraction at a curved edge.

$\overline{R}$. Nevertheless, the matching of the phase functions at the edge

$$\psi_i(Q_E) = \psi_r(Q_E) = \psi_d(Q_E)$$

is a necessary condition, which yields some useful information about the solution. After a few simple manipulations one obtains

$$\hat{e} \cdot \hat{s}' = \hat{e} \cdot \hat{s}^r = \hat{e} \cdot \hat{s} \tag{13}$$

and from this follows Keller's *law of edge diffraction:* the angle of diffraction β_d is equal to the angle of incidence β_0, so that the diffracted rays emanating from Q_E form a cone whose half-angle is β_0 and whose axis is the tangent to the edge. The incident ray and the ray reflected from the surface at Q_E also lie on the cone of the diffracted rays. The equality between the first and third quantities in (13) is used to find Q_E, given the locations of the source and field points away from the edge; in some cases this must be done by a computer search procedure.

The form of the dyadic diffraction coefficient will be treated next. If an edge-fixed coordinate system is used to describe the components of the incident and diffracted fields, it has been found that the dyadic diffraction coefficient is the sum of seven dyads [18], [19] in the matrix form this means that the diffraction coefficient is a 3 × 3 matrix with 7 nonvanishing elements. However, from (5) it is apparent that if a ray-fixed coordinate system were used in place of the edge-fixed coordinate system, the diffraction coefficient would reduce to a 2 × 2 matrix, so that no more than four dyads would be required. A further reduction in the number of dyads can be anticipated if the proper ray-fixed coordinate is chosen. Recall that this kind of simplification is achieved in the case of the dyadic reflection coefficient, if the incident and reflected fields are resolved into components parallel and perpendicular to the planes of incidence and reflection, respectively, where the plane of reflection, which contains the normal to the surface and the reflected ray, coincides with the plane of incidence. Analogous planes of incidence and diffraction can be defined in the present case.

The plane of incidence for edge diffraction, referred to simply as the edge-fixed plane of incidence henceforth, contains the incident ray and the unit vector $\hat{e}$ tangent to the edge of the point of incidence Q_E. The plane of diffraction contains the diffracted ray and $\hat{e}$. These planes are depicted in Fig. 5; they are azimuthal planes with respect to the polar axis containing $\hat{e}$, and their positions can be specified by the angles ϕ' and ϕ shown in Fig. 5(b). The unit vectors $\hat{\phi}'$ and $\hat{\phi}$ are perpendicular to the edge-fixed plane of incidence and the plane of diffraction, respectively. The unit vector $\hat{s}^i \equiv \hat{s}'$ is in the direction of incidence at the edge and the unit vector $\hat{s}$ is in the direction of diffraction. The unit vectors $\hat{\beta}_0'$ and $\hat{\beta}_0$ are parallel to the edge-fixed plane of incidence and the plane of diffraction, respectively, and

$$\hat{\beta}_0' = \hat{s}' \times \hat{\phi}'$$
$$\hat{\beta}_0 = \hat{s} \times \hat{\phi}.$$

Thus the coordinates of the diffracted ray $(s, \pi - \beta_0, \phi)$ are spherical coordinates and so are the coordinates of the incident ray (s', β_0, ϕ'), except that the incident (radial) unit vector points toward the origin Q_E.

According to Keller's theory [3], the diffraction coefficient for a curved edge may be deduced from a two-dimensional canonical problem involving a straight edge, where the cylindrical surfaces which form the edge are defined by the boundary curves depicted in Fig. 5(b). In the present discussion the edge may be an ordinary edge formed by a discontinuity in the unit normal vector, an edge formed by a discontinuity in surface curvature, or an edge formed by a discontinuity in some higher order derivative of the surface.

Consider the z components of the electric and magnetic fields in the presence of this surface with an edge

$$E_z = E_z^i + E_z^r + E_z^d \tag{14a}$$
$$H_z = H_z^i + H_z^r + H_z^d \tag{14b}$$

they satisfy

$$(\nabla^2 + k^2) \begin{Bmatrix} E_z \\ H_z \end{Bmatrix} = 0 \tag{15}$$

together with the soft (Dirichlet) or hard (Neumann) bound-

ary conditions

$$E_z = 0 \tag{16}$$

or

$$\frac{\partial H_z}{\partial n} = 0 \tag{17}$$

respectively, on the boundary curve and the radiation condition at infinity. The $\partial/\partial n$ is the derivative along the normal to the boundary curve.

Starting with the high-frequency solutions for the z components of the diffracted field, substituting these into (15), and employing the methods described earlier, the asymptotic solutions may be put into the form

$$\left.\begin{matrix} E_z^d \\ H_z^d \end{matrix}\right\} \sim \left.\begin{matrix} E_z^i & D_s \\ H_z^i & D_h \end{matrix}\right\} \sqrt{\frac{\rho}{s(\rho+s)}}\, \exp(-jks) \tag{18}$$

in which D_s is referred to as the soft scalar diffraction coefficient obtained when the soft boundary condition is used, and D_h is referred to as the hard scalar diffraction coefficient obtained when the hard boundary condition is used.

Since

$$E_z^i = E_{\beta_0'}^i \sin\beta_0 \tag{19a}$$

$$H_z^i = Y_c E_{\phi'}^i \sin\beta_0 \tag{19b}$$

and similarly for the z components of the diffracted field, it follows from (18) and (19) that

$$\left.\begin{matrix} E_{\beta_0}^d \\ E_{\phi}^d \end{matrix}\right\} = - \left.\begin{matrix} E_{\beta_0'}^i & D_s \\ E_{\phi'}^i & D_h \end{matrix}\right\} \sqrt{\frac{\rho}{s(\rho+s)}}\, \exp(-jks) \tag{20}$$

consequently, the dyadic diffraction coefficient for an ordinary (or higher order) edge in a perfectly conducting surface can be expressed simply as the sum of two dyads

$$\overline{D} = - \hat{\beta}_0' \hat{\beta}_0 D_s - \hat{\phi}' \hat{\phi} D_h \tag{21}$$

to first order. Since D_s and D_h are the ordinary scalar diffraction coefficients which occur in the diffraction of acoustic waves which encounter soft or hard boundaries, we see the close connection between electromagnetics and acoustics at high frequencies. Also, it follows that the high-frequency diffraction by more general edge structures, and by thin curved wires can be described in the form given by (11) and (21).

The balance of this paper is concerned with finding expressions for D_s and D_h which can be used in the transition regions adjacent to shadow and reflection boundaries in the case of diffraction by an ordinary edge. Recently, Keller and Kaminetzky [20] and Senior [21] have obtained expressions for the scalar diffraction coefficients in the case of diffraction by an edge formed by a discontinuity in surface curvature, and Senior [22] has given the dyadic (or matrix) diffraction coefficient in an edge-fixed coordinate system. Keller and Kaminetzkey [20] also have given expressions for the scalar diffraction coefficients in the case of higher order edges.

The diffraction by a wedge will be considered first; the wedge edge serves as a good introduction to the more difficult subject of diffraction by a curved edge. As noted earlier, the dyadic diffraction coefficient can be found from the asymptotic solution of several canonical problems, which involve the illumination of the edge by different wavefronts. It is not difficult to generalize the resulting expressions for the scalar diffraction coefficients to the case of illumination by an arbitrary wavefront.

IV. The Wedge

When a plane, cylindrical, or conical electromagnetic wave is incident on a perfectly conducting wedge, the solution may be formulated in terms of the components of the electric and magnetic field parallel to the edge; we will take these to be the z components. In the case of a spherical wave it is convenient to use the z components of the electric and magnetic vector potentials. These z components may be represented by eigenfunction series obtained by the method of Green's functions. The Bessel and Hankel functions in the eigenfunction series are replaced by their integral representations and the series are then summed leaving the integral representations. Integral representations for the other field components in the edge-fixed coordinate system are then found from the z (or edge) components, except in the case of the incident spherical wave, where the integral representations of the field components are obtained from the z components of the vector potentials. These integrals are approximated asymptotically by the Pauli–Clemmow method of steepest descent [23], and the leading terms are retained. The field components are then transformed to the ray-fixed coordinate system described previously. The resulting expression for the diffracted field can be written in the form of (11) which makes it possible to deduce the dyadic diffraction coefficient $\overline{D}$. The asymptotic solutions outlined in this paragraph are presented in detail [8].

Summarizing the results given in [8]

$$E^d(s) \sim E^i(Q_E) \cdot \overline{D}(\hat{s}, \hat{s}')\, A(s) \exp(-jks) \tag{22}$$

in which $A(s)$ describes how the amplitude of the field varies along the diffracted ray;

$$A(s) = \begin{cases} \dfrac{1}{\sqrt{s}}, & \text{for plane, cylindrical, and conical wave incidence (in the case of cylindrical wave incidence, } s \text{ is replaced by } r = s\sin\beta_0, \text{ the perpendicular distance to the edge)} \\ \sqrt{\dfrac{s'}{s(s'+s)}}, & \text{for spherical wave incidence.} \end{cases} \tag{23}$$

It follows from (12) that $\rho = \rho_e^i$ for the wedge. In the case of plane, cylindrical, and conical waves ρ_e^i is infinite and in the case of spherical waves $\rho_e^i = s'$. The dyadic diffraction coefficient $\overline{D}(\hat{s}, \hat{s}')$ has the form given in (21), which supports the assumptions leading to that equation.

If the field point is not close to a shadow or reflection boundary, the scalar diffraction coefficients [3]

$$D_{s,h}(\phi, \phi'; \beta_0) = \frac{\exp[-j(\pi/4)] \sin\pi/n}{n\sqrt{2\pi k}\sin\beta_0} \cdot \left[\frac{1}{\cos\pi/n - \cos[(\phi-\phi')/n]} \mp \frac{1}{\cos\pi/n - \cos[(\phi+\phi')/n]}\right] \tag{24}$$

for all four types of illumination, which is important, because the diffraction coefficient should be independent of the edge illumination away from shadow and reflection boundaries where the plane surfaces forming the wedge are $\phi = 0$ and $\phi = n\pi$. The wedge angle is $(2-n)\pi$; see Fig. 5(b). This ex-

pression becomes singular as shadow or reflection boundaries are approached, which further aggravates the difficulties at these boundaries resulting from the discontinuities in the incident or reflected fields. Combining (11), (21), and (24), it is seen that outside the transition regions the diffracted field is of order $k^{-1/2}$ with respect to the incident and reflected fields. In (24) and in equations to follow the upper sign applies to D_s and the lower to D_h.

Grazing incidence, where $\phi' = 0$ or $n\pi$ must be considered separately. In this case $D_s = 0$, and the expression for D_h given by (24) must be multiplied by a factor of 1/2. The need for the factor of 1/2 may be seen by considering grazing incidence to be the limit of oblique incidence. At grazing incidence the incident and reflected fields merge, so that one-half the total field propagating along the face of the wedge toward the edge is the incident field and the other half is the reflected field. Nevertheless in this case it is clearly more convenient to regard the total field as the "incident" field. The factor of 1/2 is also apparent if the analysis is carried out with $\phi' = 0$ or $n\pi$.

To simplify the discussion, the wedge angle has been restricted so that $1 < n \leqslant 2$; however, the solution for the diffracted field may be applied to an interior wedge where $0 < n < 1$. The diffraction coefficient vanishes when $\sin \pi/n = 0$; hence for $n = 1$, the entire plane, $n = 1/2$, the interior right angle, $n = 1/M$, $M = 3, 4, 5, \cdots$, interior acute angles, the boundary value problem can be solved exactly in terms of the incident field and a finite number of reflected fields, which may be determined from image theory. Moreover as $n \to 0$, even with the presence of a nonvanishing diffracted field, the phenomenon is increasingly dominated by the incident and reflected fields.

Returning now to the subject of exterior edge diffraction, the regions of rapid field change adjacent to the shadow and reflection boundaries are referred to as *transition regions*. In the transition regions the magnitude of the diffracted field is comparable with the incident or reflected field, and since these fields are discontinuous at their boundaries, the diffracted fields must be discontinuous at shadow and reflection boundaries for the total field to be continuous there.

An expression for the dyadic diffraction coefficient of a perfectly conducting wedge which is valid both within and outside the transition regions [8] is provided by (21) with

$$D_{s,h}(\phi, \phi'; \beta_0) = \frac{-\exp[-j(\pi/4)]}{2n\sqrt{2\pi k}\sin\beta_0} \times \left[\cot\left(\frac{\pi + (\phi - \phi')}{2n}\right) F[kL\,a^+(\phi - \phi')] + \cot\left(\frac{\pi - (\phi - \phi')}{2n}\right) F[kL\,a^-(\phi - \phi')] \mp \left\{\cot\left(\frac{\pi + (\phi + \phi')}{2n}\right) F[kL\,a^+(\phi + \phi')] + \cot\left(\frac{\pi - (\phi + \phi')}{2n}\right) F[kL\,a^-(\phi + \phi')]\right\}\right] \quad (25)$$

where

$$F(X) = 2j\sqrt{X}\exp(jX)\int_{\sqrt{X}}^{\infty} \exp(-j\tau^2)\,d\tau \quad (26)$$

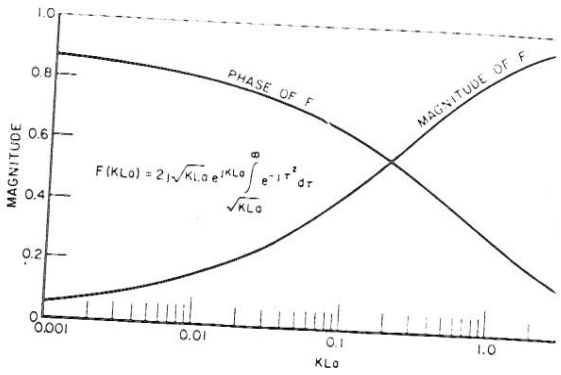

Fig. 6. Transition function.

in which one takes the principal (positive) branch of t root, and

$$a^{\pm}(\beta) = 2\cos^2\left(\frac{2n\pi N^{\pm} - (\beta)}{2}\right)$$

in which $N^{\pm}$ are the integers which most nearly sa equations

$$2\pi n N^{+} - (\beta) = \pi$$

and

$$2\pi n N^{-} - (\beta) = -\pi$$

with

$$\beta = \phi \pm \phi'.$$

It is apparent that N^+, N^- each have two values.

The preceding expression for the soft (s) and hard fraction coefficients contains a transition function F fined by (26), where it is seen that $F(X)$ involves a integral. The magnitude and phase of $F(X)$ are shown 6, where $X = kLa$. When X is small

$$F(X) \simeq \left[\sqrt{\pi X} - 2X\exp\left(j\frac{\pi}{4}\right) - \frac{2}{3}X^2\exp\left(-j\frac{\pi}{4}\right)\right] \cdot \exp\left[j\left(\frac{\pi}{4} + X\right)\right]$$

and when X is large

$$F(X) \sim \left(1 + j\frac{1}{2X} - \frac{3}{4}\frac{1}{X^2} - j\frac{15}{8}\frac{1}{X^3} + \frac{75}{16}\frac{1}{X^4}\right).$$

If the arguments of the four transition functions in (25 ceed 10, it follows from the above equation that the tran functions can be replaced by unity, and (25) reduces to

L is a distance parameter, which was determined for se types of illumination. It was found that

$$L = \begin{cases} s\sin^2\beta_0, & \text{for plane-wave incidence} \\ \dfrac{rr'}{r + r'}, & \text{for cylindrical-wave incidence} \\ \dfrac{ss'}{s + s'}\sin^2\beta_0, & \text{for conical- and spherical-wave incidences} \end{cases}$$

where the cylindrical wave of radius r' is normally incident the edge, and r is the perpendicular distance of the field po from the edge. A more general expression for L, valid for

pression becomes singular as shadow or reflection boundaries are approached, which further aggravates the difficulties at : boundaries resulting from the discontinuities in the incident or reflected fields. Combining (11), (21), and (24), it is seen that outside the transition regions the diffracted field is of order $k^{-1/2}$ with respect to the incident and reflected fields. In (24) and in equations to follow the upper sign applies to D_s and the lower to D_h.

Grazing incidence, where $\phi' = 0$ or $n\pi$ must be considered separately. In this case $D_s = 0$, and the expression for D_h given by (24) must be multiplied by a factor of 1/2. The need for the factor of 1/2 may be seen by considering grazing incidence to be the limit of oblique incidence. At grazing incidence the incident and reflected fields merge, so that one-half the total field propagating along the face of the wedge toward the edge is the incident field and the other half is the reflected field. Nevertheless in this case it is clearly more convenient to regard the total field as the "incident" field. The factor of 1/2 is also apparent if the analysis is carried out with $\phi' = 0$ or $n\pi$.

To simplify the discussion, the wedge angle has been restricted so that $1 < n \leqslant 2$; however, the solution for the diffracted field may be applied to an interior wedge where $0 < n < 1$. The diffraction coefficient vanishes when $\sin \pi/n = 0$; hence for $n = 1$, the entire plane, $n = 1/2$, the interior right angle, $n = 1/M$, $M = 3, 4, 5, \cdots$, interior acute angles, the boundary value problem can be solved exactly in terms of the incident field and a finite number of reflected fields, which may be determined from image theory. Moreover as $n \to 0$, even with the presence of a nonvanishing diffracted field, the phenomenon is increasingly dominated by the incident and reflected fields.

Returning now to the subject of exterior edge diffraction, the regions of rapid field change adjacent to the shadow and reflection boundaries are referred to as *transition regions*. In the transition regions the magnitude of the diffracted field is comparable with the incident or reflected field, and since these fields are discontinuous at their boundaries, the diffracted fields must be discontinuous at shadow and reflection boundaries for the total field to be continuous there.

An expression for the dyadic diffraction coefficient of a perfectly conducting wedge which is valid both within and outside the transition regions [8] is provided by (21) with

$$D_{s,h}(\phi, \phi'; \beta_0) = \frac{-\exp[-j(\pi/4)]}{2n\sqrt{2\pi k}\sin\beta_0} \times \left[\cot\left(\frac{\pi + (\phi - \phi')}{2n}\right) F[kL\,a^+(\phi - \phi')] + \cot\left(\frac{\pi - (\phi - \phi')}{2n}\right) F[kL\,a^-(\phi - \phi')] \mp \left\{\cot\left(\frac{\pi + (\phi + \phi')}{2n}\right) F[kL\,a^+(\phi + \phi')] + \cot\left(\frac{\pi - (\phi + \phi')}{2n}\right) F[kL\,a^-(\phi + \phi')]\right\}\right] \quad (25)$$

where

$$F(X) = 2j\sqrt{X}\exp(jX)\int_{\sqrt{X}}^{\infty} \exp(-j\tau^2)\,d\tau \quad (26)$$

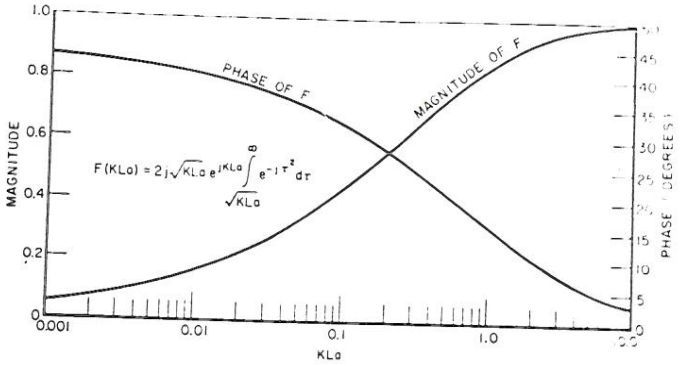

Fig. 6. Transition function.

in which one takes the principal (positive) branch of the square root, and

$$a^{\pm}(\beta) = 2\cos^2\left(\frac{2n\pi N^{\pm} - (\beta)}{2}\right) \quad (27)$$

in which $N^{\pm}$ are the integers which most nearly satisfy the equations

$$2\pi n N^{+} - (\beta) = \pi \quad (28a)$$

and

$$2\pi n N^{-} - (\beta) = -\pi \quad (28b)$$

with

$$\beta = \phi \pm \phi'. \quad (29)$$

It is apparent that N^+, N^- each have two values.

The preceding expression for the soft (s) and hard (h) diffraction coefficients contains a transition function $F(X)$ defined by (26), where it is seen that $F(X)$ involves a Fresnel integral. The magnitude and phase of $F(X)$ are shown in Fig. 6, where $X = kLa$. When X is small

$$F(X) \simeq \left[\sqrt{\pi X} - 2X\exp\left(j\frac{\pi}{4}\right) - \frac{2}{3}X^2\exp\left(-j\frac{\pi}{4}\right)\right] \cdot \exp\left[j\left(\frac{\pi}{4} + X\right)\right] \quad (30)$$

and when X is large

$$F(X) \sim \left(1 + j\frac{1}{2X} - \frac{3}{4}\frac{1}{X^2} - j\frac{15}{8}\frac{1}{X^3} + \frac{75}{16}\frac{1}{X^4}\right). \quad (31)$$

If the arguments of the four transition functions in (25) exceed 10, it follows from the above equation that the transition functions can be replaced by unity, and (25) reduces to (24).

L is a distance parameter, which was determined for several types of illumination. It was found that

$$L = \begin{cases} s\sin^2\beta_0, & \text{for plane-wave incidence} \\ \dfrac{rr'}{r + r'}, & \text{for cylindrical-wave incidence} \\ \dfrac{ss'}{s + s'}\sin^2\beta_0, & \text{for conical- and spherical-wave incidences} \end{cases} \quad (32)$$

where the cylindrical wave of radius r' is normally incident on the edge, and r is the perpendicular distance of the field point from the edge. A more general expression for L, valid for an

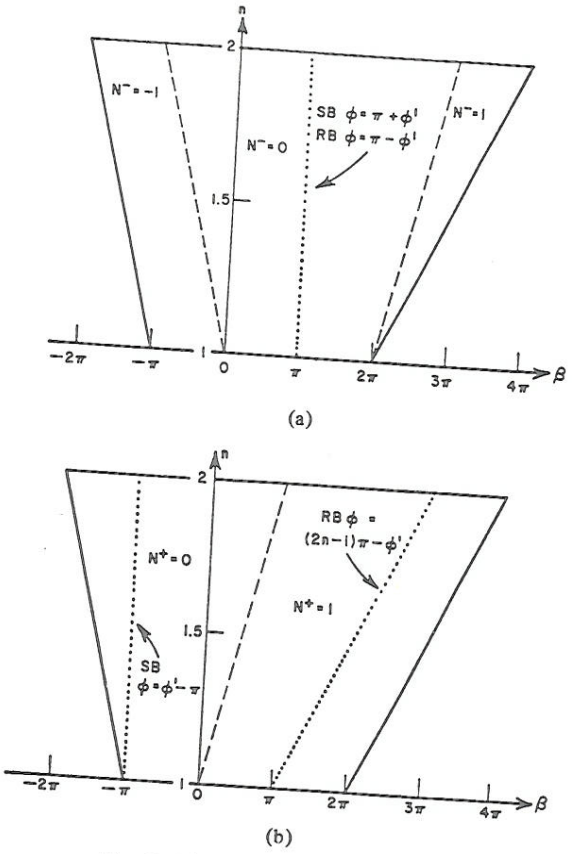

Fig. 7. N^+, N^- as functions of β and n.

TABLE I

	The cotangent is singular when	value of N at the boundary
$\cot\left(\frac{\pi+(\phi-\phi')}{2n}\right)$	$\phi=\phi'-\pi$, a SB surface $\phi=0$ is shadowed	$N^+=0$
$\cot\left(\frac{\pi-(\phi-\phi')}{2n}\right)$	$\phi=\phi'+\pi$, a SB surface $\phi=n\pi$ is shadowed	$N^-=0$
$\cot\left(\frac{\pi+(\phi+\phi')}{2n}\right)$	$\phi=(2n-1)\pi-\phi'$, a RB reflection from surface $\phi=n\pi$	$N^+=1$
$\cot\left(\frac{\pi-(\phi+\phi')}{2n}\right)$	$\phi=\pi-\phi'$, a RB reflection from surface $\phi=0$	$N^-=0$

arbitrary wavefront incident on the straight edge, will be determined later.

The large parameter in the asymptotic approximation used to find $D_{s,h}$ is kL. For incident plane waves the approximation has been found to be accurate if $kL > 1.0$, unless n is close to one, then kL should be >3.

$a^{\pm}(\beta)$ is a measure of the angular separation between the field point and a shadow or reflection boundary. The plus and minus superscripts are associated with the integers N^+ and N^-, respectively, which are defined by (28a, b). For exterior edge diffraction $N^+ = 0$ or 1 and $N^- = -1$, 0, or 1. The values of $N^{\pm}$ as functions of n and $\beta = \phi \pm \phi'$ are depicted in Figs. 7(a) and 7(b); these integers are particularly important near the shadow and reflection boundaries shown as dotted lines in the figures. It is seen that $N^{\pm}$ do not change abruptly with aspect ϕ near these boundaries, which is a desirable property.

The trapezoidal regions bounded by the solid straight lines represent the permissible values of β for $0 \leqslant \phi, \phi' \leqslant n\pi$ with $1 \leqslant n \leqslant 2$.

At a shadow or reflection boundary of the cotangent functions in the expression for $D_{s,h}$ given by (25) becomes singular; the other three remain bounded. The location of each boundary at which each cotangent becomes singular is presented compactly in Table I. In the neighborhood of the shadow or reflection boundary

$$\beta = 2\pi n N^{\pm} \mp (\pi - \epsilon) \tag{33}$$

where ϵ is positive in the region illuminated by the incident or reflected field. The $\pm$ superscript of N is directly associated with the $\mp$ sign in (33) and the $\pm$ sign in the argument of the cotangent in (34). Employing (30), it can be shown that

$$\cot\left(\frac{\pi \pm \beta}{2n}\right) F[kL\, a^{\pm}(\beta)] \simeq n\left[\sqrt{2\pi kL}\ \operatorname{sgn}\epsilon - 2kL\epsilon \exp\left(j\frac{\pi}{4}\right)\right] \exp\left(j\frac{\pi}{4}\right) \tag{34}$$

for ϵ small. It is clear that the preceding expression is finite but discontinuous at the shadow and reflection boundaries. These discontinuities compensate the discontinuity in the incident or reflected field at these boundaries, as will be shown in the paragraphs to follow.

Since the discontinuity in the geometrical-optics field at a shadow or reflection boundary is compensated separately by one of the four terms in the diffraction coefficient, there is no problem in calculating the field when two boundaries are close to each other or coincide. This occurs when $\phi' = 0$ or $n\pi$ and when ϕ' is close to $n\pi/2$ with $n \simeq 1$. The shadow and reflection boundaries are real if they occur in physical space, which is in the angular range from 0 to $n\pi$; outside this range they are virtual boundaries. If a virtual boundary is close to the surface of the wedge, as it is when ϕ' is close to π or $(n-1)\pi$, its transition region may extend into physical space near the wedge and significantly affect the calculation of the field there. The value of N^+ or N^- at each boundary is included in Table I for convenience as noted earlier, this is a stable quantity in the transition regions.

The high-frequency approximation for the total field being considered here is the sum of the geometrical-optics field and asymptotic approximation of the diffracted field. It is convenient to give the components of these fields in the ray-fixed coordinate system described earlier; hence it will be necessary to transform the components of the reflected field given in the first section to this coordinate system. We will begin by carrying out this transformation, which is facilitated by employing matrix notation.

From (7) and (8) the reflected electric field

$$\begin{bmatrix} E_{\parallel}^r \\ E_{\perp}^r \end{bmatrix} \sim \begin{bmatrix} 1 & 0 \\ 0 & -1 \end{bmatrix} \begin{bmatrix} E_{\parallel}^i \\ E_{\perp}^i \end{bmatrix} f(s) \tag{35}$$

where the subscripts $\parallel$ and $\perp$ denote components parallel and perpendicular to the ordinary plane of incidence, respectively, and

$$f(s) = \sqrt{\frac{\rho_1^i \rho_2^i}{(\rho_1^i + s)(\rho_2^i + s)}} \exp(-jks). \tag{36}$$

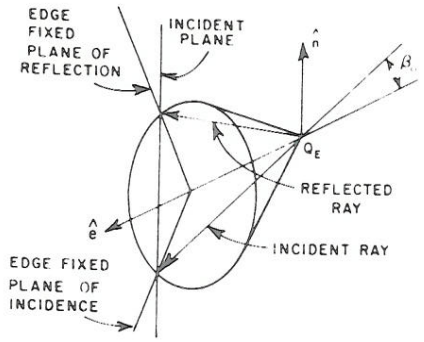

Fig. 8. Edge-fixed planes of incidence and reflection.

Note that for the plane surfaces forming the wedge $\rho_1^r = \rho_1^i$, $\rho_2^r = \rho_2^i$, where ρ_1^i, ρ_2^i are the principal radii of curvature of the incident wavefront at the point of reflection. Equation (35) may be written more compactly as

$$E^r \sim RE^i f(s). \tag{37}$$

The ordinary plane of incidence and the edge-fixed plane of incidence intersect along the incident ray passing through Q_E. The ordinary plane of incidence, the edge-fixed plane of reflection, and the cone of diffracted rays intersect at the ray reflected from Q_E. The edge-fixed plane of reflection contains the tangent to the edge and the ray reflected from Q_E. These planes and their lines of intersection are depicted in Fig. 8.

Let the angle between the edge-fixed plane of incidence and the ordinary plane of incidence be $-\alpha$. It is easily shown that angle between the edge-fixed plane of reflection and the ordinary plane of incidence is α. The components of the incident electric field parallel and perpendicular to the edge-fixed plane of incidence are given by

$$E^{i'} = T(-\alpha)\, E^i \tag{38}$$

where the components of E^i are parallel and perpendicular to the ordinary plane of incidence and

$$T(-\alpha) = \begin{bmatrix} \cos\alpha & -\sin\alpha \\ \sin\alpha & \cos\alpha \end{bmatrix}. \tag{39}$$

From (37), the reflected electric field

$$E^r \sim RE^i f(s)\, H(\epsilon) \tag{40}$$

in the neighborhood of the reflection boundary, where

$$H(\epsilon) = \tfrac{1}{2}(1 + \operatorname{sgn}\epsilon) \tag{41}$$

is the unit step function.

The components of the reflected field parallel and perpendicular to the edge-fixed plane of reflection are given by

$$T(\alpha)\, E^r = [T(\alpha)\, RT(-\alpha)^{-1}]\ [T(-\alpha)\, E^i]\, f(s)\, H(\epsilon). \tag{42}$$

From (37) and R as given in (7),

$$T(\alpha)\, RT(-\alpha)^{-1} = R \tag{43}$$

hence from (38), (41), (42), and (43)

$$\begin{bmatrix} E^r_{\beta_0} \\ E^r_{\phi} \end{bmatrix} \sim \frac{1}{2} \begin{bmatrix} 1 & 0 \\ 0 & -1 \end{bmatrix} \begin{bmatrix} E^i_{\beta_0'} \\ E^i_{\phi'} \end{bmatrix} f(s)\,(1 + \operatorname{sgn}\epsilon). \tag{44}$$

The diffraction field close to the reflection boundary at $\phi = \pi - \phi'$ is given by (11) together with (25) and (34)

$$\begin{bmatrix} E^d_{\beta_0} \\ E^d_{\phi} \end{bmatrix} \sim \frac{-1}{2} \begin{bmatrix} 1 & 0 \\ 0 & -1 \end{bmatrix} \begin{bmatrix} E^i_{\beta_0'} \\ E^i_{\phi'} \end{bmatrix} \cdot \frac{\sqrt{L}}{\sin\beta_0} \sqrt{\frac{\rho_e^i}{s(\rho_e^i + s)}}\, \exp(-jks)\, \operatorname{sgn}\epsilon$$

+ terms which are continuous at this boundary. (45)

For the total field to be continuous at the reflection boundary, the sum of the discontinuous terms in (44) and (45) must vanish; hence

$$-\frac{\sqrt{L}}{\sin\beta_0} \sqrt{\frac{\rho_e^i}{s(\rho_e^i + s)}}\, \exp(-jks) + f(s) = 0 \tag{46}$$

so that the distance parameter

$$L = \frac{s(\rho_e^i + s)\, \rho_1^i\, \rho_2^i \sin^2\beta_0}{\rho_e^i(\rho_1^i + s)\,(\rho_2^i + s)}. \tag{47}$$

The behavior of the incident and diffracted fields at the shadow boundary $\phi = \pi + \phi'$ may be treated in the same manner. After passing beyond Q_E, the electric field of the incident ray in the neighborhood of the shadow boundary is

$$\begin{bmatrix} E^i_{\beta_0} \\ E^i_{\phi} \end{bmatrix} \sim \frac{1}{2} \begin{bmatrix} -1 & 0 \\ 0 & -1 \end{bmatrix} \begin{bmatrix} E^i_{\beta_0'} \\ E^i_{\phi'} \end{bmatrix} f(s)\,(1 + \operatorname{sgn}\epsilon). \tag{48}$$

The diffracted field close to this shadow boundary is

$$\begin{bmatrix} E^d_{\beta_0} \\ E^d_{\phi} \end{bmatrix} \sim \frac{1}{2} \begin{bmatrix} 1 & 0 \\ 0 & 1 \end{bmatrix} \begin{bmatrix} E^i_{\beta_0'} \\ E^i_{\phi'} \end{bmatrix} \cdot \frac{\sqrt{L}}{\sin\beta_0} \sqrt{\frac{\rho_e^i}{s(\rho_e^i + s)}}\, \exp(-jks)\, \operatorname{sgn}\epsilon$$

+ terms which are continuous at this boundary. (49)

For the total field to be continuous at the shadow boundary, the sum of the discontinuous terms in (48) and (49) must vanish, and again it is seen that L is given by (47). Equation (47) is also obtained when the leading term in the high-frequency approximation for the total field is made to be continuous at the other shadow and reflection boundaries. Also (47) reduces to (32) for the several types of incident waves for which formal asymptotic solutions were derived. We conclude, therefore, that the expression for L given by (47) is correct when the wedge is illuminated by an incident field with an arbitrary wavefront whose principal radii of curvature are ρ_1^i and ρ_2^i.

Since kL is the large parameter in the asymptotic approximation, β_0 cannot be arbitrarily small, which precludes grazing and near grazing incidence along the edge.

The commentary on (24) in the case of grazing incidence along the surface of the wedge also applies to (25), i.e., the diffraction coefficient D_h is multiplied by a factor of 1/2 and the diffraction coefficient $D_s = 0$.

If $n = 1$ or 2, it is apparent from (27) and the integral values of $N^{\pm}$ that

$$a^{\pm}(\beta) = a(\beta) = 2\cos^2\beta/2. \tag{50}$$

Thus

$$\cot\left(\frac{\pi+\beta}{2n}\right)F[kLa^+(\beta)] + \cot\left(\frac{\pi-\beta}{2n}\right)F[kLa^-(\beta)]$$
$$= \left[\cot\left(\frac{\pi+\beta}{2n}\right) + \cot\left(\frac{\pi-\beta}{2n}\right)\right]F[kLa(\beta)]$$
$$= \frac{-2\sin\pi/n}{\cos\pi/n - \cos\beta/n}\,F[kLa(\beta)]. \tag{51}$$

The edge vanishes for $n = 1$ and the boundary surface is simply a perfectly conducting plane of infinite extent. It is seen that the diffraction coefficients and diffracted field vanish for this case as expected. If $n = 2$ the wedge becomes a half-plane and

$$D_{s,h}(\phi,\phi';\beta_0) = \frac{-\exp[-j(\pi/4)]}{2\sqrt{2\pi k}\sin\beta_0} \cdot \left\{\frac{F[kLa(\phi-\phi')]}{\cos[(\phi-\phi')/2]} \mp \frac{F[kLa(\phi+\phi')]}{\cos[(\phi+\phi')/2]}\right\} \tag{52}$$

which can be written in the form

$$D_{s,h}(\phi,\phi';\beta_0) = \frac{-\exp[j(\pi/4)]}{\sin\beta_0}\sqrt{\frac{L}{\pi}}\left[f(kL,\phi-\phi') \cdot \exp\left[j2kL\cos^2\left(\frac{\phi-\phi'}{2}\right)\right]\operatorname{sgn}(\pi+\phi'-\phi) \mp f(kL,\phi+\phi')\exp\left[j2kL\cos^2\frac{(\phi+\phi')}{2}\right] \cdot \operatorname{sgn}(\pi-\phi'-\phi)\right] \tag{53}$$

where

$$f(kL,\beta) = \int_{\sqrt{2kL}\,|\cos\beta/2|}^{\infty} \exp(-j\tau^2)\,d\tau \tag{54}$$

is a Fresnel integral.

When the diffraction coefficients given by (53) are used to calculate the fields diffracted by hard or soft half-planes illuminated by a plane wave, $L = s\sin^2\beta_0$ and the result is in agreement with a solution obtained by Sommerfeld [24]. Since Sommerfeld's solution is an exact solution, we know that our solution is exact for this case too. If these half-planes are illuminated by a cylindrical wave whose radius of curvature is r', $L = rr'/(r+r')$ in which r is the perpendicular distance from the field point to the edge, and our solution reduces to an approximate solution deduced by Rudduck [26] from the work of Obha [27] and Nomura [28]. Rudduck and his coworkers have applied this solution to a number of two-dimensional antenna and scattering problems with good accuracy.

In this section on diffraction by wedges, diffraction coefficients have been obtained which may be used at all aspects surrounding the wedge, including its surfaces and the transition regions adjacent to shadow and reflection boundaries.

V. General Wedge Configurations

The treatment of wedge diffraction in the preceding section is extended to more general edge configurations here. Our construction of the solution is again based on Keller's method of the canonical problem. The justification of the method is that high-frequency diffraction like high-frequency reflection is a local phenomenon, and locally one can approximate an edge geometry by a wedge whose surfaces are tangent to the surfaces forming the edge at the point of diffraction. We note that the reflection coefficient for a curved surface derived in Section I could have been found by this method, choosing as the canonical problem the reflection of plane waves from a plane surface, which is tangent to the curved surface at the reflection point. With these assumptions, the results of the preceding section can be applied directly to the general edge problem which may involve both curved edges and curved surfaces. It will be seen that it is only necessary to modify the expressions for the distance parameter L, which appear in the arguments of the transition functions.

In the present treatment we do not show that our solution can be matched to a boundary layer solution valid at and near the edge. It would be desirable to carry this out to confirm the validity of our solution and possibly to obtain additional terms in the asymptotic approximation. Ahluwalia [13] has used a boundary layer solution in this way to obtain an asymptotic expansion for the scalar field diffracted by a curved edge; however his representation of the total field differs from the one given here. It does not appear as separate contributions from the incident, reflected, and diffracted fields.

A. Plane and Curved Screens

The diffraction by a curved edge in a plane screen affords the simplest example of curved edge diffraction. The scalar diffraction coefficients are given by (52) or (53) and since $\rho = \rho_e^i$ on both the shadow and reflection boundaries, L is the distance parameter given by (47). At aspects other than incidence and reflection, ρ within the square root term of (11) is calculated from (12). As in the case of the wedge, we obtain a high-frequency approximation at all points surrounding the edge, which are not too close to the edge or to caustics of the diffracted field.

The diffraction by a straight or curved edge in a curved screen ($n = 2$) is next in the order of increasing difficulty. Whenever the surface forming the edge is curved, the region near it is dominated by surface diffraction phenomena, which is particularly important on the convex side. On the convex side of the curved screen there are surface ray modes, also known as creeping waves, which shed energy tangentially as they propagate along the surface. As a result of this, the radiation leakage is significant in a considerable region near the surface. On the concave side of the curved screen, we have bound modes that do not attenuate as they propagate; these modes are known as whispering-gallery modes. Both types of modes are excited by an illuminated edge in a curved surface; however the creeping waves also may be excited at grazing incidence. As mentioned earlier, surface diffraction phenomena have been neglected in the present treatment; hence the region between the convex surface and the boundary ES between the edge diffracted and surface diffracted rays must be excluded. The boundary ES is formed by the intersection of the cone of diffracted rays and the plane tangent to the surface at Q_E; in general it does not lie in the ordinary plane of incidence. In addition, the transition region adjacent to the boundary must be excluded. This region from which the field and source points are to be excluded appears as the shaded portion of Fig. 9, where all rays and boundaries are shown projected on the plane perpendicular to the

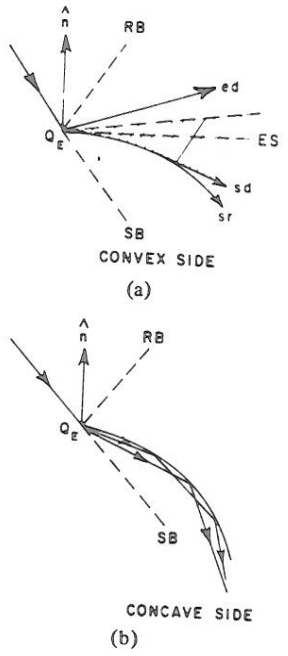

Fig. 9. Diffraction at the edge of a curved screen.

edge at Q_E. It should be noted that in general the projection of the surface ray sr does not coincide with the intersection of the boundary surface S and the plane of projection.

On the concave side the whispering-gallery effect can be described approximately by geometrical optics in the form of a series of reflected waves whose rays form cords along the concave reflecting surface as indicated in Fig. 9. Note that there is a caustic on each cord. As glancing incidence is approached, the cord length diminishes and the description of the phenomenon in terms of a sequence of reflections breaks down; the geometrical-optics analysis must be truncated at this point. If the errors resulting from this truncation are not serious, the radiation from the concave side can be included in the present analysis.

In this case $n = 2$, and the scalar diffraction coefficients in (21) are given by

$$D_{s,h}(\phi, \phi'; \beta_0) = \frac{-\exp[-j(\pi/4)]}{2\sqrt{2\pi k}\sin\beta_0} \cdot \left\{ \frac{F[kL^i a(\phi - \phi')]}{\cos[(\phi - \phi')/2]} \mp \frac{F[kL^r a(\phi + \phi')]}{\cos[(\phi + \phi')/2]} \right\} \quad (55)$$

in which the first term is discontinuous at the shadow boundary, whereas the second is discontinuous at the reflection boundary. Unlike the reflection from a plane surface, the divergence or spreading of the wave reflected from a curved surface is different from that of the incidence wave; hence the radii of curvature of the reflected and diffracted wavefronts at the reflection boundary are distinct from the radii of curvature of the incident and diffracted wavefronts at the shadow boundary. Employing arguments similar to those used to find the distance parameter for the wedge

$$L^i = \frac{s(\rho_e^i + s)\,\rho_1^i \rho_2^i \sin^2\beta_0}{\rho_e^i(\rho_1^i + s)(\rho_2^i + s)} \quad (56a)$$

$$L^r = \frac{s(\rho_e^r + s)\,\rho_1^r \rho_2^r \sin^2\beta_0}{\rho_e^r(\rho_1^r + s)(\rho_2^r + s)} \quad (56b)$$

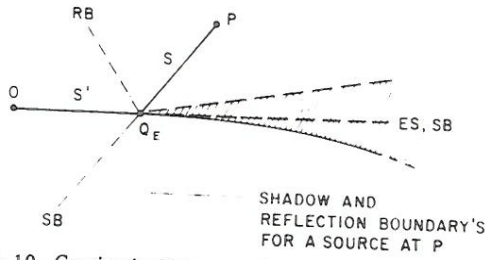

Fig. 10. Grazing incidence on the edge of a curved screen.

where ρ_e^i, ρ_1^i, ρ_2^i are defined as before, ρ_1^r and ρ_2^r are the principal radii of curvature of the reflected wavefront at Q_E, and from (12)

$$\frac{1}{\rho_e^r} = \frac{1}{\rho_e^i} - \frac{2(\hat{n}\cdot\hat{n}_e)(\hat{s}'\cdot\hat{n})}{a\sin^2\beta_0}. \quad (57)$$

As ϕ' approaches π we approach grazing incidence as shown in Fig. 10. Then since $\rho_1^r \rho_2^r \to 0$, $L^r \to 0$ and (55) can no longer be used to calculate the scalar diffraction coefficients. Under these circumstances the shadow and reflection boundaries usually lie within the shaded region in Fig. 10, and the transition regions associated with edge diffraction overlap those associated with surface diffraction. If the field and source points are both sufficiently far from the edge, we may set the transition functions in (55) equal to unity. On the other hand, for the field point or source point close to the edge or for both points close to the edge, we may be able to use reciprocity (see [25]) to calculate the field at P in Fig. 10, if the distance parameters for a unit source located at P are large enough.

B. Curved Wedges

We conclude by finding the scalar diffraction coefficients for a curved (or straight) edge in an otherwise smooth curved surface. Again we seek diffraction coefficients which can be used in the transition regions associated with the shadow and reflection boundaries of this structure. Both surfaces forming the edge may be convex, both surfaces may be concave, one surface may be convex and the other concave, or one surface may be plane and the other convex or concave.

First, let us consider the simple case which occurs when the illuminated surface forming the curved edge is plane, as it may be at the base of a cylinder or cone. For this configuration the reflected field is found directly from the incident field, as it is in the case of the wedge, e.g., it may be easily deduced from image theory. Thus the scalar diffraction coefficients are found directly from (25) and the distance parameter from (47). The calculated diffracted field may not be accurate close to the shadowed surface if surface diffraction phenomena are significant.

The more general problem where the illuminated surface is curved is closely related to the diffraction by an edge in a curved screen which has just been discussed; for example, the field point and source point must not be too close to a convex surface and the case of grazing incidence must be treated separately.

We introduce the wedge tangent to the boundary surfaces of the curved edge at Q_E. The boundary ES is formed by the intersection of this wedge with the cone of diffracted rays. Away from the boundary ES on the cone of diffracted rays the scalar diffraction coefficients are given by (25), except

that distance parameter L in the argument of each of the four transition functions may be different. As before, L is found in each case by requiring the total field to be continuous at each shadow and reflection boundary.

It is seen from Figs. 7(a) and (b) that N^+, N^- associated with the shadow boundaries at $\phi' - \pi, \phi' + \pi$ are different from zero only at angular distances greater than π from these boundaries. When this angular distance exceeds π the field point is usually outside the transition region in question, unless kL is small. In view of the assumptions involved in extending the wedge solution to the curved edge, the validity of the approximation is in question for such small values of kL, so they are excluded here. These considerations and analogous considerations lead us to set the $N^{\pm}$ equal to the values they have in Table I.

Then

$$D_{s,h}(\phi,\phi';\beta_0) = \frac{\exp[-j(\pi/4)]}{2n\sqrt{2\pi k}\sin\beta_0} \times \left[\frac{2\sin(\pi/n)\,F[kL^i a(\phi-\phi')]}{\cos(\pi/n)-\cos[(\phi-\phi')/n]} \pm \left\{\cot\left(\frac{\pi+(\phi+\phi')}{2n}\right)F[kL^{rn}a^+(\phi+\phi')] + \cot\left(\frac{\pi-(\phi+\phi')}{2n}\right)F[kL^{r0}a(\phi+\phi')]\right\}\right] \quad (58)$$

in which $a(\beta) = 2\cos^2\beta/2$ and $a^+(\beta) = 2\cos^2(2\pi n - \beta)/2$.

Again employing arguments similar to those used in the preceding section to find the distance parameters for the wedge, one finds that L^i is given by (56a), and that L^{r0}, L^{rn} are given by (56b). The additional superscripts 0 and n denote that the dii of curvature are calculated at the reflection boundaries $\cdot - \phi'$ and $(2n-1)\pi - \phi'$, respectively.

Although the reasoning employed to find the distance parameters is the same as that used in the preceding cases, namely, that the total field be continuous at the shadow and reflection boundaries, a problem arises which was not encountered earlier. For a given aspect of incidence it is clear that only two of the boundaries associated with the three transition functions exist, the other boundary is outside real space. Since neither the field or source points are permitted close to grazing incidence at $\phi' = 0$ or $n\pi$, it is reasonable to set the transition function, which is associated with the boundary located outside the interval $0 < \phi < n\pi$, equal to one.

At grazing incidence $\phi' = \pi$ or $(n-1)\pi$ for which L^{r0} or L^{rn} vanish, the scalar diffraction coefficients are calculated by the same procedure used for the curved screen at grazing incidence $\phi' = \pi$.

In the far zone where $s \gg$ the principal radii of curvature ρ_1, ρ_2 of the incident and reflected wavefronts at Q_E and the radius of curvature ρ of the diffracted wavefront at Q_E in the directions of incidence and reflection, (47), (56a), and (56b) simplify to the form

$$L = \frac{\rho_1\rho_2\sin^2\beta_0}{\rho_e} \quad (59)$$

the appropriate superscripts are omitted here for notational simplicity.

interesting case occurs if there is a caustic of the incident, ı. cted or diffracted wave on a shadow or reflection boundary. The radii of curvature ρ_1, ρ_2, or ρ associated with such a caustic are negative, and L may be either negative or positive. If L is positive, the presence of caustics at these boundaries presents no difficulty, except at points near the caustic itself. On the other hand if L is negative, there is a problem because the transition function has two branches each with an imaginary argument. We will restrict our attention to the situation where all the caustics on the boundary lie between the field point and the edge; this may occur in far-zone field calculations for example.

It can be shown (see [25, appendix II]) that if L is negative the incident (or reflected) field has one more caustic on the shadow (or reflection) boundary than does the diffracted field. This means that the phase of the transition function must change by an additional $\pi/2$ as one moves from a point outside the transition region to the boundary, so that the transition function must have a total phase variation of $3\pi/4$ instead of the $\pi/4$ phase variation shown in Fig. 6. An examination of the two branches of the transition function at the boundary and outside the transition region reveals that they do not have the proper behavior.

When a curved strip is illuminated by a plane wave from its concave side, there is a caustic of the reflected field on the reflection boundaries. In treating the scattering from this strip we have found that an adequate function is provided by

$$|F(k|L|a)|\exp\{j3[\text{phase of } F(k|L|a)]\}$$

in which $F(k|L|a)$ is the ordinary transition function given by (26). (Note that L and a may have superscripts.) In spite of the fact that the preceding expression has the proper behavior outside transition regions and at shadow or reflection boundaries and also appears to yield good numerical results, it lacks theoretical justification. A satisfactory derivation of the transition function for L negative is being sought.

VI. Discussion

A dyadic diffraction coefficient has been obtained for an electromagnetic wave obliquely incident on a curved edge formed by perfectly conducting curved or plane surfaces. Unlike the edge diffraction coefficient of Keller's original theory, this diffraction coefficient is valid in the transition regions of the shadow and reflection boundaries. Although the diffraction coefficient has been given in dyadic form in the earlier sections, it can also be represented in matrix form, so that the high-frequency diffracted electric field can be written

$$\begin{bmatrix} E^d_{\beta_0} \\ E^d_{\phi} \end{bmatrix} = \begin{bmatrix} -D_s & 0 \\ 0 & -D_h \end{bmatrix} \begin{bmatrix} E^i_{\beta_0'} \\ E^i_{\phi} \end{bmatrix} \sqrt{\frac{\rho}{s(\rho+s)}}\exp(-jks) \quad (60)$$

with the high-frequency diffracted magnetic field

$$H^d = Y_c\,\hat{s} \times E^d \quad (61)$$

in which D_s, D_h are given by

1) (58) for the curved wedge (general case),
2) (55) for an edge in a curved screen,
3) (52) or (53) for a curved or straight edge in a plane screen with ρ given by (12)
4) (25) for the wedge.

It is pointed out in Section IV that the scalar diffraction coefficients in cases 1) and 2) are not valid at aspects of incidence and diffraction close to grazing on a convex surface forming the edge at the point of diffraction. Work is in progress to remove this limitation. Also grazing incidence on a plane surface is a special case which requires the introduction of a factor of 1/2 when calculating the diffracted field.

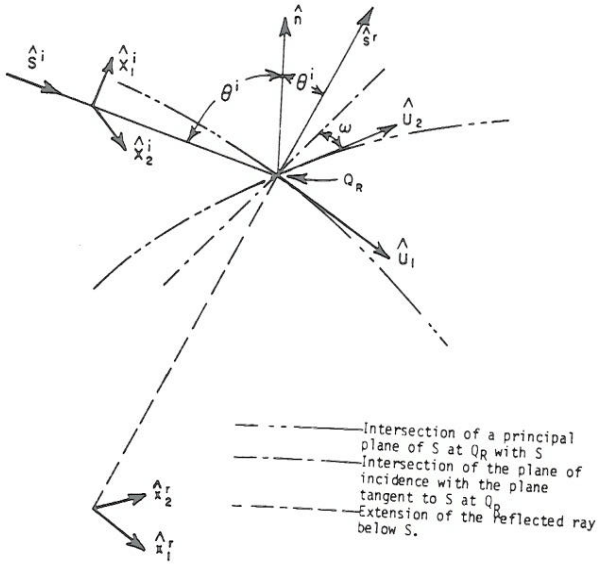

Fig. 11. Geometry for the description of the wavefront reflected from the curved surface S.

The large parameters (in the asymptotic approximation) are kL or kL^i, kL^r; hence when these are small our GTD representation of the diffracted field is no longer valid. Thus source or field points close to the edge (s or s' small) must be excluded; also aspects of incidence close to edge-on incidence (β_0 small) must be excluded. Edge-on incidence is a separate phenomenon, which has been discussed in [29] and [30].

Outside of the transition regions where the arguments of the transition functions are greater than 10, the expressions for the scalar diffraction coefficients all simplify to (24). Usually the field point is only in one transition region at a time, so that the calculation of the diffracted field is simplified because only one of the transition functions is significantly different from unity.

One would expect the diffraction coefficients for the wedge to be more accurate than those for geometries with curved edges or surfaces because the canonical problems involve wedge diffraction. If the canonical problem involved a curved edge, one would anticipate the presence of additional terms in the asymptotic solution for the diffracted field; these higher order terms would depend upon the radius of curvature of the edge at the point of diffraction and its derivatives with respect to distance along the edge. This is verified by the work of Buchal and Keller [31] and Wolfe [32], who treated the diffraction of a scalar plane wave normally incident on a plane screen with a curved edge.

In calculating the diffracted field, it is assumed that the incident field is slowly varying at the point of diffraction, except for its phase variation along the incident ray. If the incident field is rapidly varying at the point of diffraction, it may be possible to express it as a sum of slowly varying component fields, so that the diffracted field of each component can be calculated in the usual way and the total diffracted field obtained by superposition. Alternatively, in calculating the diffracted field, one could introduce higher order terms which depend upon the spatial derivatives of the incident field at the point of diffraction. Expressions of this type were obtained by Zitron and Karp [33] in their treatment of the scattering from cylinders; they are also derived in [11].

Equation (60) cannot be used to calculate the field at a caustic of the diffracted ray. At such a caustic it is convenient to use a supplementary solution in the form of an integral representation of the field. The equivalent sources in this representation are determined from a suitable high-frequency approximation, such as geometrical optics or the GTD. In the case of an axial caustic, it is convenient to employ equivalent electric and magnetic edge currents introduced by Ryan and Peters [34]; the use of edge currents is also described in [35].

In conclusion, we note that the geometrical-optics field and our expression for the edge diffracted field are both asymptotic solutions of Maxwell's equations. The total high-frequency field is the sum of these two fields, and away from the edge it is everywhere continuous, except at caustics. Our solution reduces to known asymptotic solutions for the wedge, and it has been found to yield the first two or three terms in the asymptotic expansion of the diffracted fields of problems which can be solved differently. Furthermore, the numerical results obtained by its application to a number of examples are found to be in excellent agreement with rigorously calculated and measured values. Also we have been able to show [25] that our solution is consistent with the reciprocity principle.

Appendix I
The Caustic Distance for Reflection

The principal radii of curvature of the reflected wavefront ρ_1^r, ρ_2^r, and the principal directions (axes) of the wavefront are given in this Appendix. The plane of incidence may be different from the principal planes of the reflecting surface, so that the principal directions of the incident wavefront are quite distinct from those of the reflecting surface.

Let a wavefront be incident on a curved surface S at Q_R as shown in Fig. 11. $\hat{U}_1, \hat{U}_2$ are unit vectors in the principal directions of S at Q_R with principal radii of curvature R_1, R_2. $\hat{X}_1^i, \hat{X}_2^i$ are the principal directions of the incident wavefront at Q_R with principal radii of curvature ρ_1^i, ρ_2^i. $\hat{x}_1^r, \hat{x}_2^r$ are unit vectors perpendicular to the reflected ray; they are determined by reflecting the unit vectors $\hat{X}_1^i, \hat{X}_2^i$ in the plane tangent to S at Q_R, i.e.,

$$\hat{x}_{1,2}^r = \hat{X}_{1,2}^i - 2(\hat{n} \cdot \hat{X}_{1,2}^i)\hat{n} \tag{A-1}$$

(see Fig. 11). As will be seen, $\hat{x}_1^r, \hat{x}_2^r$ are not in the principal di-

rections of the reflected wavefront. We now define

$$Q_0^i = \begin{bmatrix} 1/\rho_1^i & 0 \\ 0 & 1/\rho_2^i \end{bmatrix} \tag{A-2}$$

$$C_0 = \begin{bmatrix} 1/R_1 & 0 \\ 0 & 1/R_2 \end{bmatrix} \tag{A-3}$$

and

$$\Theta = \begin{bmatrix} \hat{X}_1^i \cdot \hat{U}_1 & \hat{X}_1^i \cdot \hat{U}_2 \\ \hat{X}_2^i \cdot \hat{U}_1 & \hat{X}_2^i \cdot \hat{U}_2 \end{bmatrix}. \tag{A-4}$$

Deschamps [36] has shown that the curvature matrix for the reflected wavefront

$$Q^r = Q_0^i + 2(\Theta^{-1})^T C_0 \Theta^{-1} \cos\theta^i \tag{A-5}$$

in which the superscript -1 denotes the inverse matrix, the superscript T denotes the transpose matrix, and θ^i is the angle of incidence;

$$Q^r = \begin{bmatrix} Q_{11}^r & Q_{12}^r \\ Q_{12}^r & Q_{22}^r \end{bmatrix} \tag{A-6}$$

where

$$Q_{11}^r = \frac{1}{\rho_1^i} + \frac{2\cos\theta^i}{|\Theta|^2}\left[\frac{(\Theta_{22})^2}{R_1} + \frac{(\Theta_{21})^2}{R_2}\right] \tag{A-7a}$$

$$Q_{12}^r = \frac{-2\cos\theta^i}{|\Theta|^2}\left[\frac{\Theta_{22}\Theta_{12}}{R_1} + \frac{\Theta_{11}\Theta_{21}}{R_2}\right] \tag{A-7b}$$

$$Q_{22}^r = \frac{1}{\rho_2^i} + \frac{2\cos\theta^i}{|\Theta|^2}\left[\frac{(\Theta_{12})^2}{R_1} + \frac{(\Theta_{11})^2}{R_2}\right] \tag{A-7c}$$

with

$$\Theta_{jk} = \hat{X}_j^i \cdot \hat{U}_k. \tag{A-7d}$$

We have diagonalized Q^r to find its eigenvalues $1/\rho_1^r$, $1/\rho_2^r$.

$$\begin{aligned}\frac{1}{\rho_{1,2}^r} &= \frac{1}{2}\left(\frac{1}{\rho_1^i} + \frac{1}{\rho_2^i}\right) + \frac{\cos\theta^i}{|\Theta|^2} \\ &\cdot\left[\frac{(\Theta_{22})^2 + (\Theta_{12})^2}{R_1} + \frac{(\Theta_{21})^2 + (\Theta_{11})^2}{R_2}\right] \\ &\pm \frac{1}{2}\left\{\left(\frac{1}{\rho_1^i} - \frac{1}{\rho_2^i}\right)^2 + \left(\frac{1}{\rho_1^i} - \frac{1}{\rho_2^i}\right)\frac{4\cos\theta^i}{|\Theta|^2}\right. \\ &\cdot\left[\frac{(\Theta_{22})^2 - (\Theta_{12})^2}{R_1} + \frac{(\Theta_{21})^2 - (\Theta_{11})^2}{R_2}\right] \\ &+ \frac{4\cos^2\theta^i}{|\Theta|^4}\left[\left(\frac{(\Theta_{22})^2 + (\Theta_{12})^2}{R_1}\right.\right. \\ &\left.\left.\left.+ \frac{(\Theta_{21})^2 + (\Theta_{11})^2}{R_2}\right)^2 - \frac{4|\Theta|^2}{R_1 R_2}\right]\right\}^{1/2}\end{aligned} \tag{A-8}$$

which the plus sign is associated with ρ_1^r and the minus sign with ρ_2^r. This equation has the form of an elementary mirror formula, except that the reciprocal of the object distance is replaced by the mean curvature of the incident wavefront.

The incident spherical wavefront is frequently of interest; for this case it can be shown that

$$\begin{aligned}\frac{1}{\rho_{1,2}^r} &= \frac{1}{s'} + \frac{1}{\cos\theta^i}\left[\frac{\sin^2\theta_2}{R_1} + \frac{\sin^2\theta_1}{R_2}\right] \\ &\pm \sqrt{\frac{1}{\cos^2\theta^i}\left[\frac{\sin^2\theta_2}{R_1} + \frac{\sin^2\theta_1}{R_2}\right]^2 - \frac{4}{R_1 R_2}}\end{aligned} \tag{A-9}$$

in which s' is the radius of curvature of the incident wavefront at Q_R; θ_1 is the angle between the direction of the incident ray $\hat{s}^i$ and $\hat{U}_1$, and θ_2 is the angle between $\hat{s}^i$ and $\hat{U}_2$. Equation (A-9) was obtained by Kouyoumjian several years earlier using a different method.

We conclude this section by giving the eigenvectors of Q^r; these yield the principal directions of the reflected wavefront with respect to the x_1^r, x_2^r coordinates;

$$\hat{X}_1^r = \frac{[(Q_{22}^r - 1/\rho_1^r)\hat{x}_1^r - Q_{12}^r\,\hat{x}_2^r]}{\sqrt{\left(Q_{22}^r - \frac{1}{\rho_1^r}\right)^2 + (Q_{12}^r)^2}} \tag{A-10}$$

$$\hat{X}_2^r = -\hat{s}^r \times \hat{X}_1^r. \tag{A-11}$$

It should be noted that the principal directions of the wavefront are distinct from the principal directions associated with the reflection matrix; as pointed out in the text the latter are parallel and perpendicular to the plane of incidence.

Acknowledgment

The authors wish to express their thanks to Prof. L. B. Felsen for his careful review of this paper.

References

[1] J. B. Keller, "The geometric optics theory of diffraction," presented at the 1953 McGill Symp. Microwave Optics, A.F. Cambridge Res. Cent., Rep. TR-59-118 (II), pp. 207–210. 1959.
[2] —, "A geometrical theory of diffraction," in *Calculus of Variations and its Applications*, L. M. Graves, Ed. New York: McGraw-Hill, 1958, pp. 27–52.
[3] —, "Geometrical theory of diffraction," *J. Opt. Soc. Amer.*, vol. 52, pp. 116–130, 1962.
[4] M. Kline, "An asymptotic solution of Maxwell's equations," *Commun. Pure Appl. Math.*, vol. 4, pp. 225–262, 1951.
[5] D. L. Hutchins and R. G. Kouyoumjian, "Asymptotic series describing the diffraction of a plane wave by a wedge," Ohio State Univ., Columbus, Rep. 2183-3, Dec. 15, 1969, ElectroScience Lab., Dep. Elec. Eng., prepared under Contract AF 19(628)-5929 for A.F. Cambridge Res. Labs, (AFCRL-69-0412), also ASTIA Doc. AD 699 228.
[6] W. Pauli, "On asymptotic series for functions in the theory of diffraction of light," Phys. Rev., vol. 54, pp. 924–931, 1938.
[7] F. Oberhettinger, "On asymptotic series for functions occurring in the theory of diffraction of waves by wedges," *J. Math. Phys.*, vol. 34, pp. 245–255, 1956.
[8] P. H. Pathak and R. G. Kouyoumjian, "The dyadic diffraction coefficient for a perfectly-conducting wedge," ElectroScience Lab., Dep. Elec. Eng., Ohio State Univ., Columbus, Rep. 2183-4, June 5, 1970, prepared under Contract AF 19(628)-5929 for A.F. Cambridge Res. Labs. (AFCRL-69-0546), also ASTIA Doc. AD 707 827.
[9] J. J. Bowman, T. B. A. Senior, and P. L. E. Uslenghi, *Electromagnetic and Acoustic Scattering by Simple Shapes*. Amsterdam, The Netherlands: North-Holland Pub., 1969.
[10] D. S. Jones, *The Theory of Electromagnetism*. New York: Macmillan, 1964.
[11] D. S. Ahluwalia, R. M. Lewis, and J. Boersma, "Uniform asymptotic theory of diffraction by a plane screen," *SIAM J. Appl. Math.*, vol. 16, pp. 783–807, 1968.
[12] R. M. Lewis and J. Boersma, "Uniform asymptotic theory of edge diffraction," *J. Math. Phys.*, vol. 10, pp. 2291–2305.
[13] D. S. Ahluwalia, "Uniform asymptotic theory of diffraction by

the edge of a three-dimensional body," *SIAM J. Appl. Math.*, 18, pp. 287–301, 1970.
[14] J. B. Keller, R. M. Lewis, and B. D. Seckler, "Asymptotic solution of some diffraction problems," *Commun. Pure Appl. Math.*, vol. 9, pp. 207–265, 1956.
[15] R. G. Kouyoumjian, "Asymptotic high frequency methods," *Proc. IEEE*, vol. 53, pp. 864–876, Aug. 1965.
[16] I. Kay and J. B. Keller, "Asymptotic evaluation of the field at a caustic," *J. Appl. Phys.*, vol. 25, pp. 876–883, 1954.
[17] D. Ludwig, "Uniform asymptotic expansions at a caustic," *Commun. Pure Appl. Math.*, vol. 19, pp. 215–250, 1966.
[18] J. B. Keller, "Diffraction by an aperture," *J. Appl. Phys.*, vol. 28, pp. 426–444, Apr. 1957.
[19] T. B. A. Senior and P. L. E. Uslenghi, "High-frequency back-scattering from a finite cone," *Radio Sci.*, vol. 6, pp. 393–406, 1971.
[20] L. Kaminetsky and J. B. Keller, "Diffraction coefficients for higher order edges and vertices," *SIAM J. Appl. Math.*, vol. 22, pp. 109–134, 1972.
[21] T. B. A. Senior, "Diffraction coefficients for a discontinuity in curvature," *Electron. Lett.*, vol. 7, no. 10, pp. 249–250, May 20, 1971.
[22] T. B. A. Senior, "The diffraction matrix for a discontinuity in curvature," *IEEE Trans. Antennas Propagat.*, vol. AP-20, pp. 326–333, May 1972.
[23] P. C. Clemmow, "Some extensions to the method of integration by steepest descents," *Quart. J. Mech. Appl. Math.*, vol. 3, pp. 241–256, 1950.
[24] A. Sommerfeld, "Mathematische Theorie der Diffraktion," *Math. Ann.*, vol. 47, pp. 317–374, 1896.
[25] R. G. Kouyoumjian and P. H. Pathak, "The dyadic diffraction coefficient for a curved edge," ElectroScience Laboratory, Dep. Elec. Eng., Ohio State Univ., Columbus, Rep. 3001-3, Aug. 1973, prepared under Grant NGR 36-008-144 for NASA, Langley Research Center, Hampton, Va., (see Appendix III).
[26] R. C. Rudduck, "Application of wedge diffraction to antenna theory," ElectroScience Lab., Dep. Elec. Eng., Ohio State Univ., Columbus, Rep. 1691-13, June 30, 1965, prepared under Grant NsG-448 for NASA.
[27] Y. Obha, "On the radiation patterns of a corner reflector," *IRE Trans. Antennas Propagat.*, vol. AP-11, pp. 127–132, Mar. 1963.
[28] Y. Nomura, "On the diffraction of electromagnetic waves by a perfectly reflecting wedge," *Res. Inst., Tohoku* Univ., Sendai, Japan, Sci. Reps., Series B, vol. 1 and 2, no. 1, pp. 1–24, 1951.
[29] C. E. Ryan and L. Peters, Jr., "A creeping-wave analysis of the edge-on echo area of discs," *IEEE Trans. Antennas Propagat.* (Lett.), vol. AP-16, pp. 274–275, Mar. 1968.
[30] T. B. A. Senior, "Disc scattering at edge-on incidence," *IEEE Trans. Antennas Propagat.*, vol. AP-17, pp. 751–756, Nov. 1969.
[31] R. N. Buchal and J. B. Keller, "Boundary layer problems in diffraction theory," *Commun. Pure Appl. Math.*, vol. 13, pp. 85–114, 1960.
[32] P. Wolfe, "Diffraction of a scalar wave by a plane screen," *SIAM J. Appl. Math.*, vol. 14, pp. 577–599, 1966.
[33] N. Zitron and S. N. Karp, "Higher-order approximation in multiple scattering. I. Two-dimensional scalar case," *J. Math. Phys.*, vol. 2, pp. 394–406, 1961.
[34] C. E. Ryan, Jr., and L. Peters, Jr., "Evaluation of edge-diffracted fields including equivalent currents for the caustic regions," *IEEE Trans. Antennas Propagat.*, vol. AP-17, pp. 292–299, May 1969.
[35] P. A. J. Ratnasiri, R. G. Kouyoumjian, and P. H. Pathak, "The wide angle side lobes of reflector antennas," Report 2183-1, 23 March 1970, ElectroScience Lab., Dep. Elec. Eng., Ohio State Univ., Columbus, prepared under Contract AF 19(628)-5929 for A.F. Cambridge Res. Labs. (AFCRL-69-0413), also ASTIA Doc. AD 707 105.
[36] G. A. Deschamps, "Ray techniques in electromagnetics," *Proc. IEEE*, vol. 60, pp. 1022–1035, Sept. 1972.